Pulse-Controlled Topologically Protected Quantum Batteries

Jin Yang(杨瑾)[1], Biao Xiong(熊标)[1*], Jibing Liu(刘继兵)[2,1], Houguo Yu(余厚果)[1], Dehua Liu(刘德华)[1], Feng Mei(梅锋)[3,4*], and Chuanjia Shan(单传家)[1*]

[1]*College of Physics and Electronic Science, Hubei Normal University, Huangshi 435002, China*
[2]*Hubei Engineering Institute, Huangshi 435006, China*
[3]*State Key Laboratory of Quantum Optics and Quantum Optics Devices, Institute of Laser Spectroscopy, Shanxi University, Taiyuan, Shanxi 030006, China*
[4]*Collaborative Innovation Center of Extreme Optics, Shanxi University, Taiyuan, Shanxi 030006, China*

(Received xxx; accepted manuscript online xxx)

Remote charging in the field of quantum batteries is particularly appealing because it minimizes interference between the charger and the battery, making it a subject of considerable interest. Here, we propose a robust remote charging protocol for quantum batteries based on a pulse-controlled superconducting qubit chain. By dynamically modulating the pulse-mediated couplings, we realize chiral-symmetry-protected energy transfer from the charger to the battery. We show that the charging process suppresses energy backflow due to the pulse control, and remains robust against pulse imperfections due to the chiral symmetry of the system. Moreover, the energy stored in the battery at the target time is almost fully extractable, and the protocol remains effective over a moderate range of chain lengths. To further accelerate charging, we optimize the pulse shape and elucidate the underlying physical mechanism. Our pulse-controlled topological quantum battery protocol provides a versatile framework for implementing remote topological charging and establishes a theoretical foundation for designing optimal-control strategies to enhance quantum battery performance.

Keywords: Quantum battery; Superconducting qubit; Quantum control; Topological protection

DOI: 10.1088/0256-307X/42/x/xxxxxx

Introduction—Quantum batteries (QBs), as a class of innovative energy storage devices, harness quantum resources such as coherence and entanglement to achieve potential advantages in storage capacity and charging power [1–7]. In contrast to conventional chemical batteries, QBs can be seamlessly incorporated into quantum architectures via dipole-dipole couplings, photon-mediated interactions, or other forms of light-matter interaction, thereby offering a flexible energy source for quantum technologies [8]. Over the past decade, significant theoretical breakthroughs have been made in the development of QBs, including the introduction of rigorous performance metrics such as stored energy and maximum extractable work (ergotropy) [9]. Various mechanisms have been proposed to enhance QB performance, encompassing the adiabatic evolution protocol [10], the indirect charging scheme mediated by intermediate states [11,12], the combined effects of beam-splitter and parametric amplification [13], the collective charging effect based on Dicke or Tavis-Cummings models [14–16], coherent ergotropy ratio optimization [17,18], and the Mpemba effect [19,20]. In parallel, experimental efforts have realized fundamental proof-of-principle validations of QBs across multiple platforms, most notably in superconducting circuits and trapped-ion systems [21–24].

However, in the practical implementation of QBs, the performance is inevitably compromised by several critical factors, such as energy backflow from the battery to the charger, environment-induced decoherence, and perturbations due to random system noise. Consequently, a central challenge in transitioning QBs from proof-of-principle to practical applications is to enhance performance under the influence of these factors. To address the issue of energy backflow, recent research has introduced a nonreciprocal QB scheme, which fundamentally prevents backflow losses by achieving entirely unidirectional energy transfer [25–31]. To mitigate the adverse effects of environment-induced decoherence, various reservoir engineering strategies have been proposed. These include continuous energy supply through structured reservoirs with bound states [32,33], utilization of the non-Markovian effect to significantly improve performance [34–39], interference engineering in giant-atom systems [40] and reservoir-assisted charging with quantum feedback control [41,42] or squeezing [43].

Moreover, time-dependent quantum control has been employed in various QB protocols for different purposes [23,44–46]. However, the presence of noise in classical control fields inevitably degrades QB per-

*Corresponding authors. Email: bx_hbnu@163.com; meifeng@sxu.edu.cn; cjshan@hbnu.edu.cn
©2026 Chinese Physical Society and IOP Publishing Ltd. All rights, including for text and data mining, AI training, and similar technologies, are reserved.

formance. This degradation is especially severe for large-scale remote charging of many-body systems, as the required time-dependent control involves a large number of control fields, each subject to fluctuations. How one can achieve robust QB charging against classical control field noise in remote many-body systems remains an open challenge.

Topology, as a fundamental concept in many-body systems, provides a powerful framework for understanding and engineering robust quantum phenomena, benefiting from the protection of topologically nontrivial structures [47–50]. Recent advances in topological photonics have opened promising avenues for enhancing the robustness of quantum optical effects. In the context of QBs, the concept of topological QBs has been proposed [51], where bound states in the topological system enable almost complete energy transfer, and the presence of a dark state together with a topologically robust dressed bound state renders the battery immune to single-sublattice dissipation. Separately, a $\mathcal{PT}$-symmetric SSH QB has been proposed [52], in which topology and non-Hermiticity cooperate to yield enhanced charging dynamics. Both schemes rely on static control fields with no extra control, and thus inevitably suffer from energy backflow during the charging process. Motivated by these pioneering works, we introduce time-dependent control into topological QBs to suppress energy backflow and enhance robustness against noise.

Superconducting quantum circuits, with chip-level programmability, fast all-electrical controls, and scalable architecture, provide a versatile solid-state platform for exploring topological effects [53–64]. Motivated by this, we propose a topological SSH-type superconducting qubit chain as a QB model, where the left and right edge states serve as the charger and the battery, respectively. By designing the couplings as cosine-type pulses, we realize a remote charging channel that exhibits negligible energy backflow in the adiabatic regime and is robust against noise in the control fields. Furthermore, we optimize the control protocol by introducing tan-type pulses, which significantly accelerate the charging process. Since our protocol constrains the maximum value of the coupling pulses and does not require precise control of the pulses, while remaining robust even in open systems, it is experimentally feasible. Unlike robust state-transfer protocols and their accelerated variants, such as Refs. [65–67], which also employ time-dependent control but focus on transfer fidelity, here we extend this approach to QBs and focus on the stored energy, the extractable work, and the signal-to-noise ratio of the charged QB. Our protocol addresses the energy backflow during charging and the instability against coupling noise, and separately clarifies the distinct roles of the pulse and the chiral symmetry in the QB protocol. These differences make our protocol complementary to, rather than a variant of, existing state-transfer schemes.

Model and Hamiltonian—We consider a one-dimensional SSH-type qubit chain consisting of N qubits, as illustrated in Fig. 1, with each unit cell containing two qubits labeled as a_x and b_x ($x = 1, 2, \ldots, m$). The Hamiltonian of the system is given by

$$\hat{H}(t) = \sum_{x=1}^{m} \left[J_1(t)\hat{\sigma}^+_{a_x}\hat{\sigma}^-_{b_x} + J_2(t)\hat{\sigma}^+_{b_x}\hat{\sigma}^-_{a_{x+1}} + \text{H.c.} \right], \tag{1}$$

where $\hat{\sigma}^+_{a_x} = |e\rangle_{a_x}\langle g|$ and $\hat{\sigma}^-_{a_x} = |g\rangle_{a_x}\langle e|$ are the raising and lowering operators for the qubit at site a_x, and similarly for b_x. The SSH model presented here applies generically to a wide range of qubit platforms. For a concrete implementation, we turn to the superconducting Xmon architecture [68], illustrated in Fig. 1(a), in which the coupler current provides continuous control over the nearest-neighbor coupling strength $J_j(t)$ ($j = 1, 2$) [69].

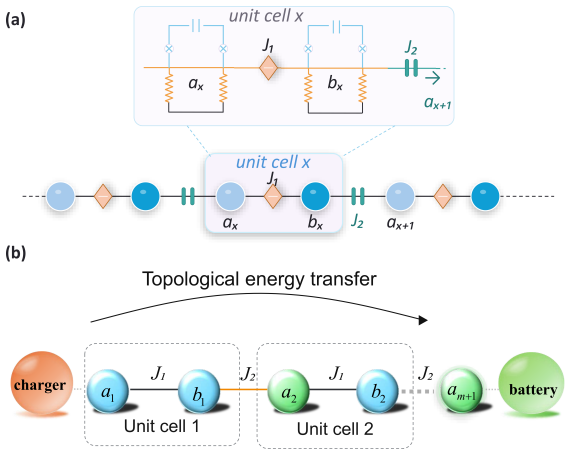

Fig. 1. (a) Schematic of the SSH-type qubit chain. Each unit cell contains two qubits a_x and b_x, with intra-cell coupling $J_1(t)$ and inter-cell coupling $J_2(t)$. (b) Schematic of the topological QB. The leftmost qubit a_1 serves as the charger, the rightmost qubit a_{m+1} as the battery, and the intermediate qubits form a topologically protected channel for energy transfer.

In our QB protocol, the leftmost qubit a_1 serves as the quantum charger, while the rightmost qubit a_{m+1} functions as the QB, as shown in Fig. 1(b). The intermediate qubits form a topologically protected channel for energy transfer. We assume that the qubit acting as the charger is initialized in the excited state, while all other qubits are prepared in their ground states. For the case of an entangled initial state, see Sec. V of the Supplementary Material. Owing to excitation-number conservation of the SSH model, the basis vectors $\{|e, g, g, \ldots\rangle, |g, e, g, \ldots\rangle, \ldots\}$ form a complete set. In this basis, the Hamiltonian takes the matrix form H_M. Further calculation reveals that

the eigenvalues of H_M are $E_-^{(m)},\ldots,E^{(0)},\ldots,E_+^{(m)}$ in ascending order, with corresponding eigenstates $|\psi\rangle_-^{(m)},\ldots,|\psi\rangle^{(0)},\ldots,|\psi\rangle_+^{(m)}$. The explicit expressions for these eigenvalues and eigenstates are given in Sec. I of the Supplemental Material. Here, we focus on the central zero eigenvalue $E^{(0)}=0$, pinned by chiral symmetry (see Sec. II of the Supplemental Material). Its eigenstate is

$$|\psi\rangle^{(0)}=\frac{1}{\sqrt{\eta_0}}\left[(-\nu)^0,0,(-\nu)^1,0,\ldots,(-\nu)^m\right]^T, \quad (2)$$

with $\nu=J_1/J_2$. It can be seen that the zero-energy eigenstate $|\psi\rangle^{(0)}\approx(1,0,0,\ldots)^T=|e,g,g,\ldots\rangle$ for $|\nu|\ll 1$, while $|\psi\rangle^{(0)}\approx(0,\ldots,0,1)^T=|g,\ldots,g,e\rangle$ for $|\nu|\gg 1$. This observation allows us to tune the value of $\nu=J_1/J_2$ such that $|\psi\rangle^{(0)}$ can be switched from the left edge state $|e,g,g,\ldots\rangle$ to the right edge state $|g,\ldots,g,e\rangle$, thereby realizing energy transition from the left-localized qubit to the right-localized qubit. In fact, there are many choices of $J_1(t)$ and $J_2(t)$ that satisfy this condition. Without loss of generality, we assume $J_1(t)$ and $J_2(t)$ as follows:

$$J_1(t)=J_0\left[1-f(t)\right], \quad J_2(t)=-J_0\left[1+f(t)\right], \quad (3)$$

where J_0 is the coupling constant, $f(t)$ satisfies $f(0)=1$ and $f(t_f)=-1$ with t_f the target time. Clearly, $|\nu(0)|=0$ and $|\nu(t_f)|=\infty$, which satisfy the above condition and thus enable the energy transfer from the left edge state to the right edge state. In the following, we utilize these topological edge states as energy carriers to realize directional energy transfer from the charger to the battery.

Topologically protected charging—To verify the above analysis, we first adopt the commonly used cosine-shaped pulses $f(t)=\cos(\pi t/t_f)$. For simplicity, we take $m=2$ (i.e., $N=5$ sites). The numerically simulated energy spectrum is presented in Fig. 2(a). It is observed that the eigenenergy $E^{(0)}$ remains zero throughout the evolution. As shown in Fig. 2(b), the corresponding zero-energy eigenstate is the left edge state $|L\rangle=|e,g,g,g,g\rangle$ at $t=0$ and the right edge state $|R\rangle=|g,g,g,g,e\rangle$ at $t=t_f$, which is consistent with the above analysis. To investigate the dynamical energy transfer from the charger to the battery through the topological passage, we introduce the energy of charger E_C and battery E_B as

$$E_C(t)=\mathrm{Tr}\left[\hat{H}_C\rho_C(t)\right], \quad E_B(t)=\mathrm{Tr}\left[\hat{H}_B\rho_B(t)\right], \quad (4)$$

where $\hat{H}_C=\omega_c\hat{\sigma}_{a_1}^+\hat{\sigma}_{a_1}^-$ and $\hat{H}_B=\omega_b\hat{\sigma}_{a_{m+1}}^+\hat{\sigma}_{a_{m+1}}^-$ are the local Hamiltonians of the charger and battery qubits, respectively, with their free frequencies $\omega_c=\omega_b$. The reduced density matrices of the charger and the battery, $\rho_C(t)$ and $\rho_B(t)$, are obtained by tracing the full density matrix $\rho(t)$ over all degrees of freedom except the charger and the battery, respectively. While E_B denotes the stored energy of the battery, its extractability is quantified by the ergotropy, i.e., the maximum extractable work, defined as

$$\mathcal{E}_B(t)=E_B(t)-\min_U \mathrm{Tr}\left[\hat{H}_B U\rho_B(t)U^\dagger\right], \quad (5)$$

where the minimization is taken over all unitary operations U acting locally on the battery. Explicitly, the ergotropy can be computed by $\mathcal{E}_B(t)=E_B(t)-\sum_j r_j\epsilon_j$, where r_j are the eigenvalues of $\rho_B(t)$ arranged in descending order, and ϵ_j are the eigenvalues of $\hat{H}_B$ arranged in ascending order.

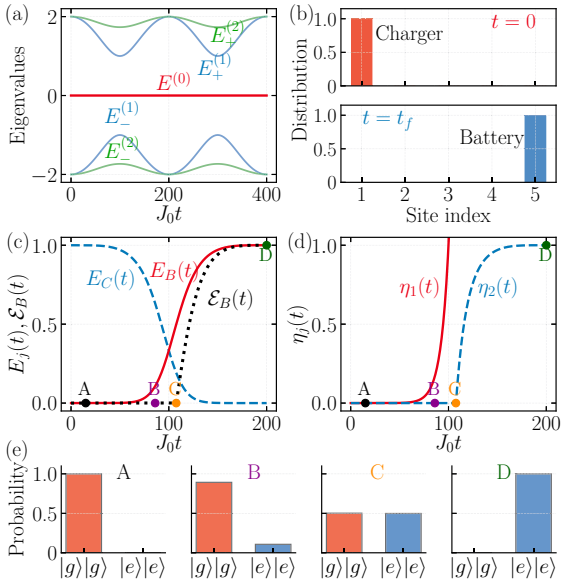

Fig. 2. (a) Energy spectrum versus t. (b) Zero-energy eigenstate at $t=0$ (upper) and $t=t_f$ (lower). (c) Time evolution of normalized charger energy $E_C(t)$ (blue dashed), battery energy $E_B(t)$ (red solid) and ergotropy $\mathcal{E}_B(t)$ (black dotted). (d) Time evolution of $\eta_1(t)$ (red solid) and $\eta_2(t)$ (blue dashed). (e) Population distributions of ρ_B in $|e\rangle$ and $|g\rangle$ at the four selected time instants A, B, C, and D marked in (c) and (d). We set $t_f=200/J_0$ and $N=5$.

In the following numerical simulations, all energies are normalized by ω_b. For notational simplicity, we write $E_j(t)$ and $\mathcal{E}_B(t)$ to denote the normalized quantity $E_j(t)/\omega_b$ and $\mathcal{E}_B(t)/\omega_b$ in the figures. In Fig. 2(c), the evolutions of normalized $E_B(t)$, $E_C(t)$ and $\mathcal{E}_B(t)$ are simulated numerically. It is observed that, as the evolution proceeds, the energy of the charger decreases while that of the battery increases. At the target time $t=t_f$, all energy initially stored in the charger is completely transferred to the battery in the ideal case. Unlike the evolution of $E_B(t)$, $\mathcal{E}_B(t)$ stays zero initially, reaches a critical point C, and then grows with time in a manner similar to the stored energy. To further characterize the charging process, we define a population-transfer ratio $\eta_1(t)=E_B(t)/E_C(t)$

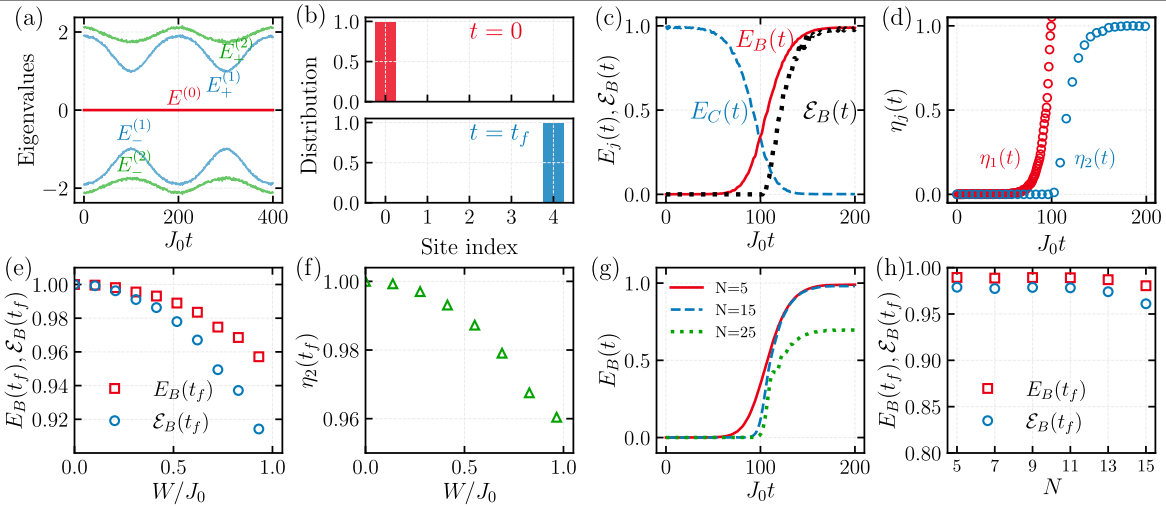

Fig. 3. (a) Energy spectrum with disorder. (b) Zero-energy eigenstate distributions at $t = 0$ (upper) and $t = t_f$ (lower). (c) Evolution of the normalized $E_C(t)$ (blue dashed), $E_B(t)$ (red solid), and $\mathcal{E}_B(t)$ (black dotted) with disorder. (d) Evolution of population-transfer ratio $\eta_1(t)$ (red circles) and extraction efficiency $\eta_2(t)$ (blue circles). (e) Normalized $E_B(t_f)$ (red squares) and $\mathcal{E}_B(t_f)$ (blue circles) versus W. (f) Extraction efficiency $\eta_2(t_f)$ versus W. (g) Evolution of normalized $E_B(t)$ for $N = 5, 15, 25$. (h) Normalized $E_B(t_f)$ (red squares) and $\mathcal{E}_B(t_f)$ (blue circles) versus N. All results are averaged over 50 trajectories, except for the data in (e), (f) and (h), where we use 100 trajectories to ensure convergence for larger W and N. We set $W/J_0 = 0.5$ in (a)-(d) and (g)-(h). Other parameters are the same as in Fig. 2.

to characterize the energy stored in the battery relative to that remaining in the charger. As shown in Fig. 2(d), $\eta_1(t)$ increases monotonically and diverges at the target time $t = t_f$, reflecting the vanishing charger energy $E_C(t_f) \to 0$. Meanwhile, $E_B(t)$ increases monotonically toward $E_C(0)$, indicating near-complete energy transfer with suppressed backflow. This suppression of backflow originates from the adiabatic pumping (see Sec. III of the Supplemental Material). Meanwhile, the extractable fraction of the stored energy is characterized by the extraction efficiency $\eta_2(t) = \mathcal{E}_B(t)/E_B(t)$, which follows a trend similar to $\mathcal{E}_B(t)$, with $\eta_2(t) = 0$ before a critical point C and increasing thereafter.

To explain why the stored energy is not extractable before the critical point, we analyze the reduced density matrix ρ_B. The off-diagonal elements of ρ_B are found to be zero throughout the evolution, so that $\rho_B = \rho_{ee}|e\rangle\langle e| + \rho_{gg}|g\rangle\langle g|$. The ergotropy is then given analytically by

$$\mathcal{E}_B(t) = \omega_b \max\{0, 2\rho_{ee}(t) - 1\}, \tag{6}$$

which is not equivalent to the stored energy $E_B(t) = \omega_b \rho_{ee}(t)$. In particular, the ergotropy vanishes for $\rho_{ee} < 1/2$ and becomes nonzero only after the population inversion is reached. Figure 2(e) shows the populations ρ_{ee} and ρ_{gg} at the four time points A, B, C, and D indicated in Figs. 2(c) and (d). At the critical point C, we have $\rho_{ee} = \rho_{gg}$. Before the critical point, as seen at points A and B, $\rho_{ee} < \rho_{gg}$, and no work can be extracted. After the critical point, $\rho_{ee} > \rho_{gg}$, which is precisely the population inversion condition for incoherent ergotropy, and thus the stored energy becomes extractable. Nevertheless, at point D ($t = t_f$), $\rho_{gg} = 0$, the state ρ_B is pure, $\eta_2(t) = 1$, confirming that the stored energy becomes completely extractable by the end of the protocol.

To verify the topologically protected nature of the charging process, we introduce disorder into the system. In our model, the primary tunable parameter is the coupling $J_i(t)$. To simulate control imperfections, we introduce disorder into the couplings $J_i(t)$ as $J_i(t) \to J_i(t) + \delta J_{i,x}$, where $\delta J_{i,x} = W\delta_{i,x}$ denotes the independent perturbation on bond x of coupling type i, with W the disorder strength and $\delta_{i,x}$ independent random variables drawn from a uniform distribution on $[-0.5, 0.5]$. In Figs. 3(a) and (b), we calculate the instantaneous energy spectrum and the corresponding zero-energy eigenstate distributions at the initial and target times, respectively, for $W/J_0 = 0.5$. In these spectral calculations, the disorder is independently resampled at each time point to examine the robustness of the zero-energy mode against coupling perturbations. As shown in Fig. 3(a), the nonzero-energy eigenvalues fluctuate due to disorder, while the zero-energy eigenvalue remains pinned at zero. Correspondingly, the zero-energy eigenstate remains strongly localized near the left edge at $t = 0$ and near the right edge at $t = t_f$, with probability distributions close to those in the ideal case shown in Fig. 2(b). This demonstrates that the edge states are robust against coupling disorder, manifesting the topological protection arising from chiral symmetry (see Sec. III of the Supplemental Material). To further examine the ro-

bustness of the charging dynamics, we consider static coupling disorder that remains fixed throughout each trajectory. As shown in Fig. 3(c), the charger energy is almost fully transferred to the battery even with weak disorder. The ergotropy evolution is nearly identical to the ideal case, indicating that the disorder with $W/J_0 = 0.5$ has negligible effect. It is precisely this topologically protected edge state that enables a disorder-robust QB protocol. Correspondingly, $\eta_1(t_f)$ becomes large, as seen in Fig. 3(d), and the extraction efficiency $\eta_2(t_f)$ remains close to 100%, demonstrating resilience against control imperfections.

We next discuss the effects of stronger disorder and larger system sizes on the battery performance. In Fig. 3(e), we simulate the normalized stored energy $E_B(t_f)$ and the ergotropy $\mathcal{E}_B(t_f)$ as a function of W. It is observed that, within a certain range of W, the presence of disorder has little effect on either quantity. However, when W becomes too large, both $E_B(t_f)$ and $\mathcal{E}_B(t_f)$ decrease with increasing W, with the extractable work being more severely affected. This indicates that disorder does alter the quantum state ρ_B of the battery. Nevertheless, even for $W/J_0 = 1$, we have $E_B(t_f)/\omega_b$ larger than 0.95 and $\mathcal{E}_B(t_f)/\omega_b$ larger than 0.9, corresponding to reductions of only 5% and 10% relative to the ideal case, respectively. This demonstrates that even strong disorder does not significantly degrade the battery performance. Moreover, although $\mathcal{E}_B(t_f)$ decreases more rapidly with W, the extraction efficiency $\eta_2(t_f)$ of the stored energy remains above 96% for $W/J_0 = 1$, as shown in Fig. 3(f), further confirming the robustness of the battery performance against disorder. In Fig. 3(g), we fix $W/J_0 = 0.5$ and simulate the evolution of the normalized $E_B(t)$ for different system sizes $N = 5$, 15, and 25. The results show that the overall evolution trends are consistent across different N, but the time at which $E_B(t)$ begins to rise significantly increases with N. Moreover, for too large N, complete energy transfer from the charger to the battery at $t = t_f$ is no longer achieved. To further investigate the finite-size effect on the stored energy and extractable work, we plot in Fig. 3(h) the normalized $E_B(t_f)$ and $\mathcal{E}_B(t_f)$ as a function of N. It is found that both $E_B(t_f)$ and $\mathcal{E}_B(t_f)$ decrease with increasing N, with the latter exhibiting a more rapid decline. Nevertheless, both quantities remain above 0.95 for $N \leq 15$, confirming that our scheme tolerates a moderately large topological chain length. For larger N, however, achieving high performance requires more precise control over the couplings to reduce the disorder strength.

Accelerating topologically protected charging—The charging speed of the battery is another important figure of merit, since a faster charging process implies a higher charging power. A further investigation shows that, since our charging protocol relies on the adiabatic following of the topological zero-energy state during the time-dependent modulation of the SSH couplings, a smaller t_f in the pulse used above violates the adiabatic condition, leading to a degradation of both the stored energy and the ergotropy (see Sec. IV of the Supplemental Material). To accelerate the topologically protected charging process, we choose an alternative control field $f(t) = \tan(\pi t/T + \alpha)/\tan(\alpha)$, with $T = \pi t_f/[2(\pi - \alpha)]$ and $\alpha = \pi/2 + \mu$, where μ modulates the flatness of the pulse shape.

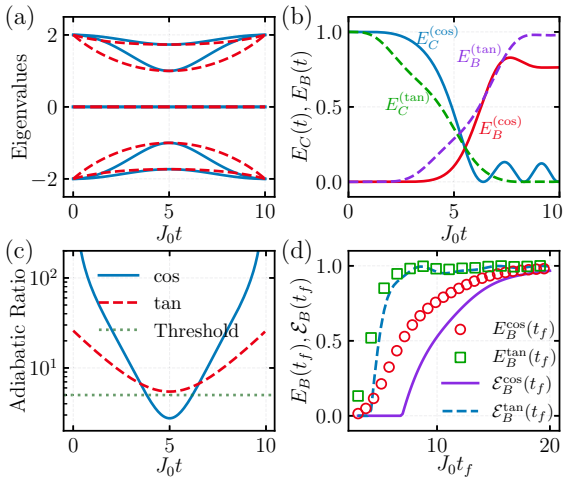

Fig. 4. (a) Energy spectra for cosine (blue solid) and tangent (red dashed) controls. (b) Normalized $E_C(t)$ and $E_B(t)$ under cosine (solid) and tangent (dashed) controls. (c) Adiabatic ratio $C(t)$ for cosine (blue solid) and tangent (red dashed) controls; the green dotted line marks the threshold. (d) Normalized $E_B(t_f)$ and $\mathcal{E}_B(t_f)$ versus t_f for both controls. We set $t_f = 10/J_0$ in (a)-(c) and $\mu = 0.8$ throughout.

For comparison, we numerically simulate the energy spectra for both the cosine-shaped and tangent-shaped pulses in Fig. 4(a), where the blue solid curve corresponds to the cosine pulse and the red dashed curve to the tangent pulse. Both spectra exhibit a zero-energy eigenvalue that remains constant in time. However, the nonzero eigenvalues show significant differences between the two cases. For the cosine-shaped pulse, the nonzero eigenvalues vary slowly near the two ends. In contrast, for the tangent-shaped pulse, the nonzero eigenvalues vary rapidly near the two ends and slowly in the middle. Dynamically, as shown in Fig. 4(b), the charging process under the tangent pulse exhibits fast evolution at early times and slow evolution in the intermediate regime. At $t = t_f$, the tangent pulse yields significantly better charging performance than the cosine pulse.

To explain this observation, we recall the adiabatic condition derived in Supplemental Material and define the adiabatic ratio

$$C = \min_{l \neq m+1} \frac{|E_{m+1} - E_l|}{\left| \left(S^{-1} \dot{S} \right)_{m+1,l} \right|}. \tag{7}$$

To satisfy the adiabatic condition, $C \gg 1$ is required. Based on our numerical results, we set a threshold of 5, with larger values indicating better adiabaticity. In Fig. 4(c), we plot the time evolution of C for both the cosine-shaped and tangent-shaped pulses. For the cosine pulse, C is large near the two ends where the variation in Fig. 4(a) is slow, but drops below the threshold of 5 in the middle of the evolution, indicating that the adiabatic condition is violated and other eigenstates become excited. As a result, at the target time, a portion of the energy remains in other bulk states. For the tangent pulse, by contrast, C remains above the threshold throughout the evolution. This result indicates improved adiabaticity for the tangent pulse, with negligible excitation of other bulk states. Consequently, the charger energy can be transferred to the battery almost completely via the topologically protected channel. This suggests that, in designing the control fields, a profile that varies rapidly at the initial and final stages, while slowly in the middle, is more favorable for satisfying the adiabatic condition and thus accelerating charging. As for the optimal control field, it could be further explored using reinforcement learning methods [70], but this is beyond the scope of the present paper. Nevertheless, the tangent-shaped pulse can accelerate the charging process compared with the cosine-shaped one. To quantify the speedup, we simulate in Fig. 4(d) the normalized stored energy and the extractable work as functions of t_f for both pulses. For the cosine pulse, a target time of at least $t_f \approx 20/J_0$ is required to achieve near-ideal charging, whereas for the tangent pulse, $t_f \approx 8/J_0$ suffices. Thus, the charging process is significantly accelerated. Moreover, since the tangent pulse satisfies the adiabatic condition better, the battery performance under the tangent pulse is more robust against the increase of chain length at the same t_f, remaining good even up to $N = 27$ (see Sec. VI of the Supplemental Material), and remains better even in the presence of dissipation and dephasing (see Sec. VII of the Supplemental Material).

Conclusions— In conclusion, we demonstrate a robust and efficient remote charging protocol based on a pulse-controlled topological superconducting qubit chain. Specifically, the chiral symmetry provides robustness against disorder, while the adiabatic pump suppresses energy backflow and enables near-perfect energy transfer from the charger to the battery. Importantly, although part of the stored energy is not extractable during the charging process, an analysis of the ergotropy confirms that the energy transferred to the battery is almost fully extractable once the charging is completed. Moreover, the charging performance remains effective up to $N = 15$ under cosine control. To accelerate charging, we optimize the pulse shape and show that the tangent pulse enhances both the stored energy and ergotropy. Owing to its better adiabaticity, the tangent pulse maintains good performance up to $N = 27$. In addition, the charging performance remains satisfactory within the range of experimentally accessible parameters in the presence of decoherence and dephasing. Overall, our results establish a flexible and robust strategy for topological quantum battery charging with suppressed energy backflow, and provide a promising framework for optimizing charging dynamics through time-dependent control.

Acknowledgements. We thank Dawei Wang of Tsinghua University for helpful discussions. This work was supported by the National Natural Science Foundation of China (Grant No. 12104141), the Natural Science Foundation Innovation-Development Joint Program of Hubei Province (Grant No. 2026AFC0003), the Key Project of the Scientific Research Program of the Department of Education of Hubei Province (Grant No. D20252503).

References

[1] Campaioli F, Gherardini S, Quach J Q, Polini M, and Andolina G M 2024 *Rev. Mod. Phys.* **96** 031001
[2] Shi H-L, Ding S, Wan Q-K, Wang X-H, and Yang W-L 2022 *Phys. Rev. Lett.* **129** 130602
[3] Liu J-X, Shi H-L, Shi Y-H, Wang X-H, and Yang W-L 2021 *Phys. Rev. B* **104** 245418
[4] Kamin F H, Tabesh F T, Salimi S, and Santos A C 2020 *Phys. Rev. E* **102** 052109
[5] Hovhannisyan K V, Perarnau-Llobet M, Huber M, and Acín A 2013 *Phys. Rev. Lett.* **111** 240401
[6] Gyhm J-Y, Šafránek D, and Rosa D 2022 *Phys. Rev. Lett.* **128** 140501
[7] Ma H-B, Xu K, Li H-G, Li Z-G, and Zhu H-J 2024 *Phys. Rev. A* **110** 022433
[8] Kurman Y, Hymas K, Fedorov A, Munro W J, and Quach J 2026 *Phys. Rev. X* **16** 011016
[9] Allahverdyan A E, Balian R, and Nieuwenhuizen T M 2004 *EPL* **67** 565
[10] Santos A C, Çakmak B, Campbell S, and Zinner N T 2019 *Phys. Rev. E* **100** 032107
[11] Farina D, Andolina G M, Mari A, Polini M, and Giovannetti V 2019 *Phys. Rev. B* **99** 035421
[12] Crescente A, Ferraro D, Carrega M, and Sassetti M 2022 *Phys. Rev. Res.* **4** 033216
[13] Liu Y-q, Yang Y-j, Liu Z, Guo B-q, Ma T-t, Zhu Z, Liu W, Zhao X, and Yu C-s 2026 *Sci. China Phys. Mech. Astron.* **69** 260312
[14] Seidov S S and Mukhin S I 2024 *Phys. Rev. A* **109** 022210
[15] Yang H-Y, Shi H-L, Wan Q-K, Zhang K, Wang X-H, and Yang W-L 2024 *Phys. Rev. A* **109** 012204
[16] Andolina G M, Farina D, Mari A, Pellegrini V, Giovannetti V, and Polini M 2018 *Phys. Rev. B* **98** 205423
[17] Song W-L, Wang J-L, Zhou B, Yang W-L, and An J-H 2025 *Phys. Rev. Lett.* **135** 020405
[18] Wang C-J and Dou F-Q 2026 *Chin. Phys. Lett.* **43** 060602
[19] Medina I, Culhane O, Binder F C, Landi G T, and Goold J 2025 *Phys. Rev. Lett.* **134** 220402
[20] Li Y, Li W, and Li X 2025 *Phys. Rev. A* **112** 032209

[21] Quach J Q, McGhee K E, Ganzer L, Rouse D M, Lovett B W, Gauger E M, Keeling J, Cerullo G, Lidzey D G, and Virgili T 2022 *Sci. Adv.* **8** eabk3160

[22] Joshi J and Mahesh T S 2022 *Phys. Rev. A* **106** 042601

[23] Hu C-K, Qiu J, Souza P J P, Yuan J, Zhou Y, Zhang L, Chu J, Pan X, Hu L, Li J, Xu Y, Zhong Y, Liu S, Yan F, Tan D, Bachelard R, Villas-Boas C J, Santos A C, and Yu D 2022 *Quantum Sci. Technol.* **7** 045018

[24] Hu C-K, Liu C, Zhao J, Zhong L, Zhou Y, Liu M, Yuan H, Lin Y, Xu Y, Hu G, Xie G, Liu Z, Zhou R, Ri Y, Zhang W, Deng R, Saguia A, Linpeng X, Sarandy M S, Liu S, Santos A C, Tan D, and Yu D 2026 *Phys. Rev. Lett.* **136** 060401

[25] Ahmadi B, Mazurek P, Horodecki P, and Barzanjeh S 2024 *Phys. Rev. Lett.* **132** 210402

[26] Sun C-Z, Wang Z-K, Yan W-B, Zhang Y-J, Man Z-X, and Cai Q-Y 2025 *Phys. Rev. A* **112** 012429

[27] Guo Y, Cao L, and Zhao J 2025 *Phys. Rev. A* **111** 063520

[28] Khan N A, Zhang X, Huang C, Liu Y, and He D 2025 *Phys. Rev. B* **112** 104318

[29] Liu B-B, Wang D-Y, Tang J, Chen G, Jing H, Su S-L, and Nori F 2026 *Phys. Rev. Lett.* **136** 253602

[30] Liu R-F, Song W-L, Yang W-L, Guan H, and An J-H 2026 *Chiral quantum batteries* (arXiv:2603.25173 [quant-ph])

[31] Liu B B, Chen R, Wu J L, Chen G, and Su S L 2026 *Phys. Rev. A* **114** 013719

[32] Bai S-Y and An J-H 2020 *Phys. Rev. A* **102** 060201(R)

[33] Song W-L, Liu H-B, Zhou B, Yang W-L, and An J-H 2024 *Phys. Rev. Lett.* **132** 090401

[34] Kamin F H, Tabesh F T, Salimi S, Kheirandish F, and Santos A C 2020 *New J. Phys.* **22** 083007

[35] Li J L, Shen H Z, and Yi X X 2022 *Opt. Lett.* **47** 5614

[36] Bhanja G, Tiwari D, and Banerjee S 2024 *Phys. Rev. A* **109** 012224

[37] Ghosh S, Chanda T, Mal S, and Sen(De) A 2021 *Phys. Rev. A* **104** 032207

[38] Xu K, Li H-G, Li Z-G, Zhu H-J, Zhang G-F, and Liu W-M 2022 *Phys. Rev. A* **106** 012425

[39] Tabesh F T, Kamin F H, and Salimi S 2020 *Phys. Rev. A* **102** 052223

[40] Yan K-X, Liu Y, Xiao Y, Lin J-H, Song J, Chen Y-H, Nori F, and Xia Y 2026 *Phys. Rev. Lett.* **136** 180401

[41] Yao Y and Shao X Q 2025 *Phys. Rev. A* **111** 062616

[42] Yin X-L, Guo M, Huang J, Lee H-w J, and Zhang G 2026 *Phys. Rev. Res.* **8** L032035

[43] Yang J, Fang S, Zhao C, Shan C, and Xiong B 2026 *Phys. Rev. Appl.* **25** 034013

[44] Mazzoncini F, Cavina V, Andolina G M, Erdman P A, and Giovannetti V 2023 *Phys. Rev. A* **107** 032218

[45] Evangelakos V, Paspalakis E, and Stefanatos D 2025 *Quantum Sci. Technol.* **10** 035024

[46] Romero S V, Chen X, and Ban Y 2026 *Phys. Rev. Lett.* **137** 050404

[47] Ozawa T, Price H M, Amo A, Goldman N, Hafezi M, Lu L, Rechtsman M C, Schuster D, Simon J, Zilberberg O, and Carusotto I 2019 *Rev. Mod. Phys.* **91** 015006

[48] Luo H, Yu P, Li G, and Yan K 2022 *Nat. Rev. Phys.* **4** 611

[49] Wang Z-Y, Chen F-J, Xi X, Gao Z, and Yang Y-H 2024 *Acta Phys. Sin.* **73** 064201

[50] Qi L, Yan Y, and Wang H F 2020 *Chin. Sci. Bull.* **65** 1076

[51] Lu Z-G, Tian G, Lü X-Y, and Shang C 2025 *Phys. Rev. Lett.* **134** 180401

[52] Zhou A-L, Xiao Y-W, Xu N, Gao L-L, Li L-J, Zhou H, Li Z-M, and Shu C-C 2026 *Phys. Rev. A* **113** 042213

[53] Cai W, Han J, Mei F, Xu Y, Ma Y, Li X, Wang H, Song Y P, Xue Z-Y, Yin Z-q, Jia S, and Sun L 2019 *Phys. Rev. Lett.* **123** 080501

[54] Qian H, Gong M, Zhang J, Guo S, Zha C, Chen F, Ye Y, Wu Y, Cao S, Ying C, Zhu Q, Huang H-L, Zhao Y, Li S, Yu J, Fan D, Wu D, Su H, Deng H, Rong H, Li Y, Zhang K, Chung T-H, Liang F, Lin J, Xu Y, Guo C, Li N, Yan K, Su F-F, Wu G, Huo Y-H, Peng C-Z, Lu C-Y, Mei F, Jia S, Zhu X, and Pan J-W 2025 *Science* **390** 930

[55] Xu S, Sun Z-Z, Wang K, Xiang L, Bao Z, Zhu Z, Shen F, Song Z, Zhang P, Ren W, Zhang X, Dong H, Deng J, Chen J, Wu Y, Tan Z, Gao Y, Jin F, Zhu X, Zhang C, Wang N, Zou Y, Zhong J, Zhang A, Li W, Jiang W, Yu L-W, Yao Y, Wang Z, Li H, Guo Q, Song C, Wang H, and Deng D-L 2023 *Chin. Phys. Lett.* **40** 060301

[56] Jin F, Jiang S, Zhu X, Bao Z, Shen F, Wang K, Zhu Z, Xu S, Song Z, Chen J, Tan Z, Wu Y, Zhang C, Gao Y, Wang N, Zou Y, Zhang A, Li T, Zhong J, Cui Z, Han Y, He Y, Wang H, Yang J-N, Wang Y, Shen J, Liu G, Deng J, Dong H, Zhang P, Li W, Yuan D, Lu Z, Sun Z-Z, Li H, Zhang J, Song C, Wang Z, Guo Q, Machado F, Kemp J, Iadecola T, Yao N Y, Wang H, and Deng D-L 2025 *Nature* **645** 626

[57] Zhang X, Jiang W, Deng J, Wang K, Chen J, Zhang P, Ren W, Dong H, Xu S, Gao Y, Jin F, Zhu X, Guo Q, Li H, Song C, Gorshkov A V, Iadecola T, Liu F, Gong Z-X, Wang Z, Deng D-L, and Wang H 2022 *Nature* **607** 468

[58] Niu J, Li Y, Zhang L, Zhang J, Chu J, Huang J, Huang W, Nie L, Qiu J, Sun X, Tao Z, Wei W, Zhang J, Zhou Y, Chen Y, Hu L, Liu Y, Liu S, Zhong Y, Lu D, and Yu D 2024 *Phys. Rev. Lett.* **132** 020601

[59] Zhang J, Huang W, Chu J, Qiu J, Sun X, Tao Z, Zhang J, Zhang L, Zhou Y, Chen Y, Liu Y, Liu S, Zhong Y, Miao J-J, Niu J, and Yu D 2025 *Phys. Rev. Lett.* **134** 070601

[60] Li C-Z, Wang A-Q, Li C, Zheng W-Z, Brinkman A, Yu D-P, and Liao Z-M 2020 *Nat. Commun.* **11** 1150

[61] Shi Y-H, Liu Y, Zhang Y-R, Xiang Z, Huang K, Liu T, Wang Y-Y, Zhang J-C, Deng C-L, Liang G-H, Mei Z-Y, Li H, Li T-M, Ma W-G, Liu H-T, Chen C-T, Liu T, Tian Y, Song X, Zhao S P, Xu K, Zheng D, Nori F, and Fan H 2023 *Phys. Rev. Lett.* **131** 080401

[62] Deng C-L, Liu Y, Zhang Y-R, Li X-G, Liu T, Chen C-T, Liu T, Lu C-W, Wang Y-Y, Li T-M, Fang C-P, Zhou S-Y, Song J-C, Xu Y-S, He Y, Liu Z-H, Huang K-X, Xiang Z-C, Wang J-C, Zheng D-N, Xue G-M, Xu K, Yu H F, and Fan H 2024 *Phys. Rev. Lett.* **133** 140402

[63] Mei F, Guo Q H, Yu Y F, Xiao L T, Zhu S L, and Jia S T 2020 *Phys. Rev. Lett.* **125** 160503

[64] Zhang J H, Mei F, Xiao L T, and Jia S T 2024 *Phys. Rev. Lett.* **132** 036603

[65] Palaiodimopoulos N E, Brouzos I, Diakonos F K, and Theocharis G 2021 *Phys. Rev. A* **103** 052409

[66] Wang Y Q, Wei M S, Liao M J, Lin Z J, Wang S L, Xu J, and Yang Y 2024 *Phys. Rev. A* **110** 063525

[67] Li K Z, Tian J Z, and Xiao L T 2025 *Phys. Rev. A* **111** 022403

[68] Mei F, Chen G, Tian L, Zhu S-L, and Jia S 2018 *Phys. Rev. A* **98** 012331

[69] Chen Y, Neill C, Roushan P, Leung N, Fang M, Barends R, Kelly J, Campbell B, Chen Z, Chiaro B, Dunsworth A, Jeffrey E, Megrant A, Mutus J Y, O'Malley P J J, Quintana C M, Sank D, Vainsencher A, Wenner J, White T C, Geller M R, Cleland A N, and Martinis J M 2014 *Phys. Rev. Lett.* **113** 220502

[70] Zhang Z, Zhao C, Liu J, Shan C, and Xiong B 2026 *Phys. Rev. A* **113** 033504